The Analysis of Circular Waveguide Phased Arrays*

By N. AMITAY and VICTOR GALINDO

(Manuscript received July 9, 1968)

In this work, a planar phased array of circular waveguides arranged in an equilateral triangular grid is analyzed. The boundary value problem is first formulated rather generally in terms of a vector two dimensional integral equation for an array of elements that are arranged in a doubly periodic grid along two skewed (nonorthogonal) coordinates. Dielectric plugs, covers, and loading, as well as thin irises at the aperture, are accounted for in the formulation. Numerical solutions are obtained by using the Ritz–Galerkin method to solve the integral equation. Excellent agreement with experimental measurements using a waveguide simulator is observed. The existence of forced surface wave phenomena in equilateral triangular grid arrays and their strong dependence upon the mode of excitation is also demonstrated. These phenomena are shown to exist at isolated points in the scan coordinates. Reflection characteristics as well as the polarization characteristics of the radiation pattern are illustrated at selected planes of scan for both linear and circular polarization excitation.

I. INTRODUCTION

The requirements of modern radar and communication systems have stimulated considerable activity in the design and use of phased array antennas. To date, the design information required for their development has been obtained from the analysis of simplified array models and from experimental data. The great speed and storage capacity of present day digital computers, however, have now made it possible to solve the planar phased array boundary value problem very accurately.[1, 2]

A general formulation of the planar phased array boundary value problem may be found. A vector two dimensional integral equation

* The work reported in this paper was supported by the U. S. Army Materiel Command under contract DA-30-069-AMC-333(Y).

for the tangential aperture field (that is, the tangential field at the planar interface between the waveguides and free space) can then be derived.

In its most general form the array elements are assumed to be arranged in a doubly periodic grid along two skewed (nonorthogonal) coordinates; and dielectric loading, covers, and plugs, as well as thin irises at the aperture plane, may be accounted for in the analysis. The possibility of multimode excitation of the array has also been included. The Ritz-Galerkin method is applied to obtain a solution for circular waveguide arrays.

Numerical solutions for the reflection characteristics of dielectric-free planar arrays of circular waveguides hexagonally arranged in a conducting ground plane have been carried out. Experimental measurements have been made which compare favorably with the results. Forced surface waves[3-11] are found to occur at isolated points in the scan coordinates and can be related to certain vector and geometrical symmetries for an equilateral triangle grid array. These surface waves (or resonances) are often difficult to locate experimentally by the use of waveguide simulators[12-14] or small test arrays. The strong dependence of these forced resonances upon the mode of excitation is also demonstrated. The reflection characteristics as well as the polarization characteristics of the radiation pattern are illustrated for various combinations of linear and circular polarization excitation of the array.

II. ANALYSIS

An infinite planar array of waveguide elements, Fig. 1, is imbedded in a conducting ground plane at its interface (plane $z = 0$) with free space. The elements are arranged in a periodic grid along the skewed (nonorthogonal) coordinates s_1 and s_2. The x and s_1 axes coincide while the s_2 axis makes an angle α with respect to the x (and s_1) axis. The element location is defined by two indices (p, q) corresponding to a physical location

$$\varrho_{pq} = pb\hat{s}_1 + qd\hat{s}_2 \tag{1}$$

where $\hat{s}_1$ and $\hat{s}_2$ are unit vectors along the s_1 and s_2 axes, while b and d represent the basic periods of the two dimensional grid. A basic periodic cell,[15] the parallelogram shown in Fig. 1, is thereby defined. If the array elements are excited uniformly in amplitude with a linear

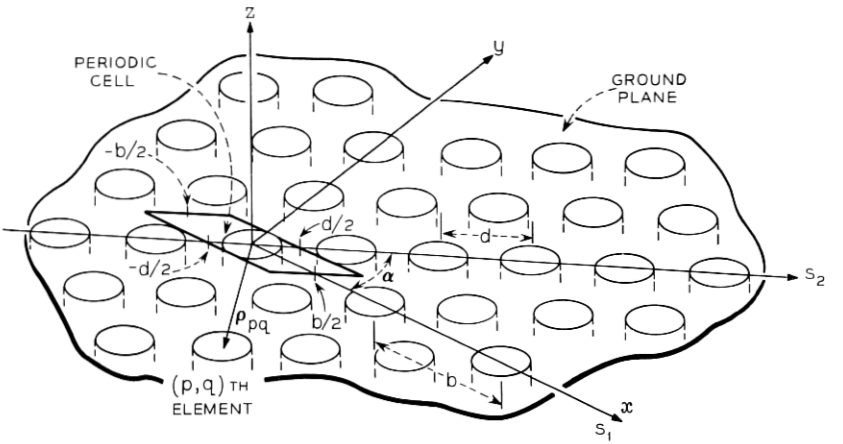

Fig. 1 — Circular waveguide array geometry.

phase taper such that the phase of the (p, q)th element is

$$\psi_{pq} = p\psi_{t_1} + q\psi_{t_2} , \tag{2}$$

then the resulting electromagnetic fields in the (p, q)th and (m, n)th periodic cells satisfy the following periodicity relationship

$$\mathbf{E}(\varrho_{pq}) = \mathbf{E}(\varrho_{mn}) \exp [i \{(m - p)\psi_{t_1} + (n - q)\psi_{t_2}\}] \tag{3}$$

where $\mathbf{E}(\varrho_{pq})$ may designate the electric or magnetic field at the (p, q)th periodic cell of the grid.* Therefore, except for a phase factor, the fields in all the cells are identical.

In order to solve the boundary value problem, the exterior (free space) fields are expressed in terms of a complete set of Floquet type solutions of Maxwell's equations $\{\Psi^v_{mn} \exp \pm iB_{mn}z\}$. These vector modes, which are functions of the steering phases ψ_{t_1} and ψ_{t_2} are derived in Appendix A. The interior $(z \leqq 0)$ fields are expressed in terms of the appropriate waveguide complete orthonormal set of vector modes $\{\Phi_i \exp \pm i\Gamma_i z\}$.† The boundary value problem is expressed in terms of an integral equation which includes the necessary continuity conditions. This equation is formulated[1] by satisfying the continuity of the transverse (to z)

* The parallelogram in Fig. 1 defines the $(p = 0, q = 0)$ cell. The (p, q)th cell is translated by pb and qd along the s_1 and s_2 axes, respectively.

† The waveguide modes are real functions and in general consist of both TE and TM modes with double subscripts. However, one can always systematically relabel these modes with a single subscript according to the increasing values of the eigenvalues.

electric and magnetic fields within a single periodic cell. As shown in Appendix B, the periodic cell consisting of the parallelogram *CDEF* of Fig. 2 can be replaced, without a loss of generality, by the parallelogram *GHIJ* (or any other periodic contiguous cell containing a complete single waveguide aperture).

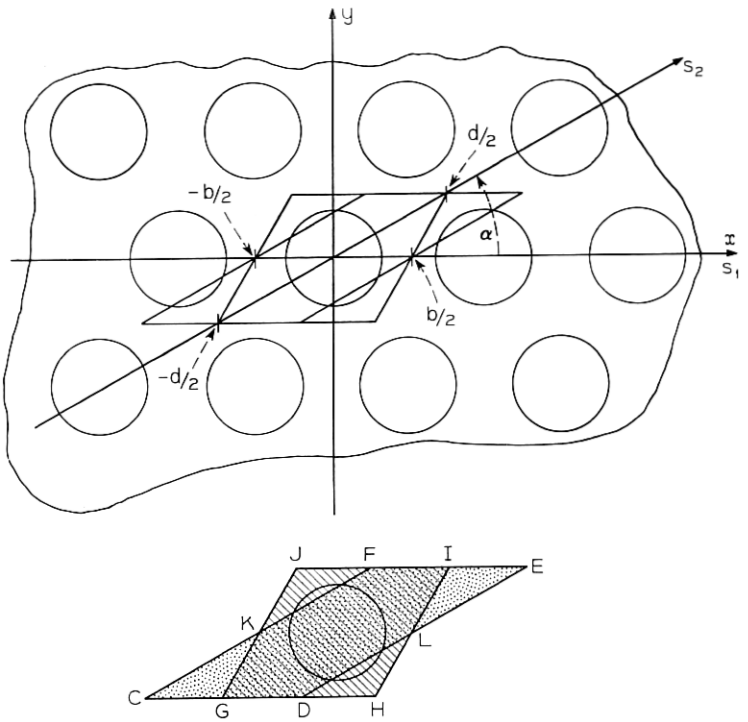

Fig. 2 — Periodic cell in skewed array geometry.

The tangential electric and magnetic fields at the array interface (**E** and **H** at $z = 0$) can be expressed in terms of a Fourier series of the complete orthonormal set of waveguide modes $\{\Phi_j\}$ for $z \leqq 0$ and by the set of Floquet type modes $\{\Psi^p_{mn}\}$ for $z \geqq 0$. Let the waveguides be excited by *any* linear combination of their propagating modes* with amplitudes $A_j (j = 1, \ldots, J$ for J propagating modes) and let the coefficients R_j represent the amplitudes of the corresponding reflected

* It is straightforward to include, if desired, *any* linear combination of both propagating and evanescent modes.

modes.* Let the coefficients D_i represent the amplitudes of the reflected evanescent modes which are generated at the aperture. Then, in terms of the waveguide modes, the electric field at $z = 0$ is given by

$$\mathbf{E}_- = \begin{cases} \sum_{i=1}^{J} (A_i + R_i)\mathbf{\Phi}_i + \sum_{i=J+1}^{\infty} D_i\mathbf{\Phi}_i & \text{(over the waveguide aperture)} \\ 0 \quad \text{(over the rest of the periodic cell).} \end{cases} \tag{4}$$

The corresponding magnetic field is

$$-\mathbf{H}_- = \begin{cases} \sum_{i=1}^{J} Y_i(A_i - R_i)\mathbf{\Phi}_i - \sum_{i=J+1}^{\infty} Y_i D_i \mathbf{\Phi}_i & \\ \qquad \text{(over the waveguide aperture)} & \\ 0 \quad \text{(over the rest of the periodic cell).} \end{cases} \tag{5}$$

where the modal admittances $\{Y_i\}$ are real for propagating modes and pure imaginary for evanescent modes. These admittances are given by[16]

$$Y_i = \frac{\Gamma_i}{\omega\mu} \quad \text{for } TE \text{ modes}; \qquad Y_i = \frac{\omega\epsilon}{\Gamma_i} \quad \text{for } TM \text{ modes} \tag{6}$$

for an exp $[-i\omega t]$ time convention with the Γ_i (the z propagation constant) being positive imaginary for evanscent modes. The tangential electric field at $z = 0^+$, expressed in terms of the Floquet type modes, is

$$\mathbf{E}_+ = \sum_{p=1}^{2} \sum_{(m)} \sum_{(n)} F_{mnp}\mathbf{\Psi}^p_{mn} \qquad \text{(over the periodic cell)} \tag{7}$$

where the superscript p designates TE($p = 1$) or TM($p = 2$) modes. The magnetic field is correspondingly given by

$$-\mathbf{H}_+ = \sum_{p=1}^{2} \sum_{(m)} \sum_{(n)} F_{mnp} Y'_{mnp} \mathbf{\Psi}^p_{mn} \tag{8}$$

where the modal admittances Y'_{mnp} are given by

$$Y'_{mn1} = \frac{B_{mn}}{\omega\mu}; \qquad Y'_{mn2} = \frac{\omega\epsilon}{B_{mn}}. \tag{9}$$

From the orthonormality of the sets $\{\mathbf{\Phi}_i\}$ and $\{\mathbf{\Psi}^p_{mn}\}$ it is clear that

$$\langle \mathbf{E}_- , \mathbf{\Phi}_i \rangle = \iint_A \mathbf{E}_- \cdot \mathbf{\Phi}_i \, da = \begin{cases} A_i + R_i & \text{for } j \leqq J \\ D_i & j > J \end{cases} \tag{10}$$

* Actually $\{R_i\}$ can represent the reflection coefficients once $\{A_i\}$ are properly normalized.

where A is the waveguide aperture, and

$$\langle \mathbf{E}_+ , \mathbf{\Psi}^p_{mn} \rangle = \iint_{\text{periodic cell}} \mathbf{E}_+ \cdot (\mathbf{\Psi}^p_{mn})^* \, da = \iint_A \mathbf{E}_+ \cdot (\mathbf{\Psi}^p_{mn})^* \, da = F_{mnp} \tag{11}$$

where the symbol * denotes the complex conjugate. Notice that $\mathbf{E}_+$ vanishes on the conducting ground plane. To insure the continuity of the tangential fields across the aperture at $z = 0$, one requires

$$\mathbf{E}_+ = \mathbf{E}_- = \mathbf{E}_t \text{ over the aperture and the periodic cell} \tag{12}$$

while

$$\mathbf{H}_+ = \mathbf{H}_- = \mathbf{H}_t \text{ over the aperture } \textit{only}. \tag{13}$$

Using the various relations, (4) through (13), one obtains an integral equation for the tangential electric field $\mathbf{E}_t$ at the array interface

$$2 \sum_{j=1}^{J} A_j Y_j \mathbf{\Phi}_j = \sum_{j=1}^{\infty} Y_j \mathbf{\Phi}_j \iint_A \mathbf{\Phi}_j \cdot \mathbf{E}_t \, da + \sum_{p=1}^{2} \sum_{(m)} \sum_{(n)} Y'_{mnp} \mathbf{\Psi}^p_{mn} \iint_A (\mathbf{\Psi}^p_{mn})^* \cdot \mathbf{E}_t \, da. \tag{14}$$

Similarly, one can obtain[1] an integral equation for $\mathbf{H}_t$ which is defined over the entire periodic cell. Under certain conditions[17] it is possible to interchange the order of summation and integration in (14) and thereby obtain the usual form of Fredholm integral equation of the first kind.

A useful method of obtaining a solution to (14) is by the application of the Ritz-Galerkin method,[18] whereby the integral equation is reduced to a linear matrix equation. Substituting (4) in (14) for $\mathbf{E}_t$ and taking the moments of (14) with respect to the set $\{\mathbf{\Phi}_i\}$, while using (10), leads to the following matrix equation

$$2 \begin{bmatrix} Y_1 A_1 \\ \vdots \\ Y_J A_J \\ 0 \\ \vdots \end{bmatrix} = |K| \begin{bmatrix} A_1 + R_1 \\ \vdots \\ A_J + R_J \\ D_{J+1} \\ \vdots \end{bmatrix}, \tag{15}$$

where $|K|$ is a square matrix with the (i, q)th element given by

$$k_{iq} = Y_i \, \delta_{iq} + \sum_{p=1}^{2} \sum_{(m)} \sum_{(n)} Y'_{mnp} C^p_{mni} C^{p*}_{mnq} . \tag{16}$$

In (16) δ_{iq} is the kroenecker delta

$$\delta_{iq} = \begin{cases} 1 & \text{if } i = q \\ 0 & \text{if } i \neq q \end{cases} \tag{17}$$

and

$$C^{p}_{mni} = \iint_{A} \tilde{\mathbf{\Psi}}^{p}_{mn} \cdot \mathbf{\Phi}_i \, da \tag{18}$$

is the coupling coefficient between the designated interior and exterior modes.*

The practicality of an accurate numerical solution or approximate analytical solution often hinges upon obtaining C^{p}_{mni} in closed form. Recently the authors[19] have obtained closed form expressions of these coupling coefficients for circular as well as coaxial waveguides.

A solution for the aperture field in terms of the coefficients of the waveguide modes is given by

$$\cdot \begin{bmatrix} A_1 + R_1 \\ \vdots \\ A_J + R_J \\ D_{J+1} \\ \vdots \end{bmatrix} = 2 \mid K \mid^{-1} \begin{bmatrix} A_1 Y_1 \\ \vdots \\ A_J Y_J \\ 0 \\ \vdots \end{bmatrix}. \tag{19}$$

The solution vector can be obtained by matrix inversion or by rapidly convergent iterative methods.[5,20] A similar procedure should be followed to obtain $\mathbf{H}_t$ except that the aperture field and the moments may be taken with respect to the set $\{\mathbf{\Psi}^{p}_{mn}\}$.

Once the aperture electric field is obtained, the input impedance and radiation properties of the array, as a function of scan, are easily obtained. The reflection coefficients are obtained directly from (19), as are the amplitudes of the evanescent modes in the waveguides. The radiation pattern of a single element in the array environment, including its polarization characteristics, can also be easily obtained.[21,22]

The addition of either a dielectric sheath or plug or both to the

* Notice that other sets of functions $\{\xi_l\}$ can be used to reduce (14) by the method of moments. However, the integrability of

$$\iint_{(A)} \mathbf{\Phi}_j \cdot \xi_l \text{ and } \iint_{(A)} \mathbf{\Psi}_{mn}{}^{p} \cdot \xi_l$$

may prove difficult depending on ξ_l. The convergence properties as a function of the order of K will also be influenced by the choice of $\{\xi_l\}$.

array, Fig. 3, does not alter the functional form of the integral equation (14). As was shown by Galindo and Wu,[3, 23] only the modal admittances in (14) have to be replaced. For the case when dielectric plugs are used, Y_j is replaced by

$$Y_j \to y_j \frac{Y_j - iy_j \tan \gamma_j t_1}{y_j - iY_j \tan \gamma_j t_1} \tag{20}$$

where y_j and γ_j are the modal admittance and propagation constants, respectively, of the Φ_j mode in the dielectric and t_1 is the dielectric plug thickness. The relation between the reflection coefficients of the propagating modes in the dielectric-free region (ϵ_0) and the aperture field is given by

$$R_j = \frac{y_j \iint_A \mathbf{E}_t \cdot \mathbf{\Phi}_j \, da - A_j \exp(-i\Gamma_j t_1)[y_j \cos \gamma_j t_1 + iY_j \sin \gamma_j t_1]}{\exp(i\Gamma_j t_1)[y_j \cos \gamma_j t_1 - iY_j \sin \gamma_j t_1]}, \tag{21}$$

the phase of R_j being referred to the aperture. Similarly, for the exterior dielectric sheath covering the array, the modal admittances are replaced by

$$Y'_{mnp} \to y'_{mnp} \frac{Y'_{mnp} - iy'_{mnp} \tan \beta_{mn} t'_1}{y'_{mnp} - iY'_{mnp} \tan \beta_{mn} t'_1}, \tag{22}$$

where y'_{mnp} and β_{mn} are the modal admittance and propagation constants, respectively, of the Ψ^p_{mn} mode in the sheath, and t'_1 is the sheath thickness. The coefficient of the mode Ψ^p_{mn} in the free space region above the sheath, F_{mnp}, is related to the aperture field by the following relation:

$$F_{mnp} = \frac{\exp(-iB_{mn} t'_1) y'_{mnp}}{y'_{mnp} \cos \beta_{mn} t_1' - iY'_{mnp} \sin \beta_{mn} t'_1} \iint_{\substack{\text{periodic} \\ \text{cell}}} \mathbf{E}_t \cdot \mathbf{\Psi}^{p*}_{mn} \, da, \tag{23}$$

the phase of F_{mnp} being referred to the aperture plane.

The integral equation formulation can be extended to the case when thin metallic irises are present at the waveguide aperture for matching purposes (see Fig. 4). The integral equation for the aperture electric field, (14), is still valid except that the integral has to be defined over the effective aperture with the result that the orthogonal relations of (10) and (11) cannot be used for the Ritz-Galerkin method of solution.* The modal coupling coefficients, (18), are still integrable in closed form

* An integral equation for the magnetic field is not valid in this case because of the discontinuity of $\mathbf{H}_t$ across the iris.

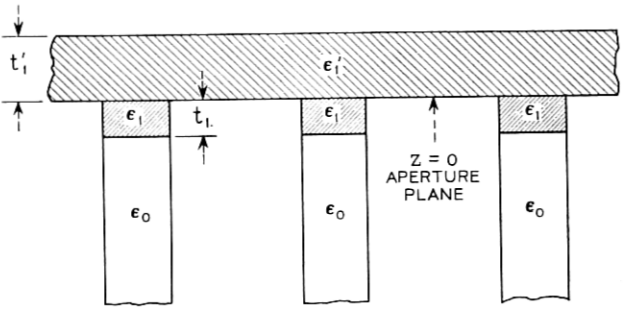

Fig. 3 — Dielectric sheath and plug geometry.

over the effective aperture if the iris is circularly symmetric. However, the matrix elements, as given by (16), do change in form when an iris is present at the aperture. As a result of the Φ_i not being orthogonal over the new effective aperture, the term $Y_i\delta_{iq}$ in (16) is replaced by an infinite sum.

Multimode excitation of waveguide antenna fields has been used for primary pattern control. Such excitations may prove useful for the reduction of mutual coupling effects.[7] They also may be used to obtain circular or elliptical polarization from two linearly polarized modes and improve the polarization characteristics of the array. In the circular waveguide array, the horizontal TE_{11} (Φ_1) and vertical TE_{11} (Φ_2) modes are degenerate (that is, they have the same z-directed propagation constant and impedance). In order to obtain a linear, elliptical or circular polarization excitation of the waveguide, one may redefine the first two modes as Φ_{1N} and Φ_{2N}:

$$\Phi_{1N} = \frac{A_1}{(|A_1|^2 + |A_2|^2)^{\frac{1}{2}}}\Phi_1 + \frac{A_2}{(|A_1|^2 + |A_2|^2)^{\frac{1}{2}}}\Phi_2 \tag{24}$$

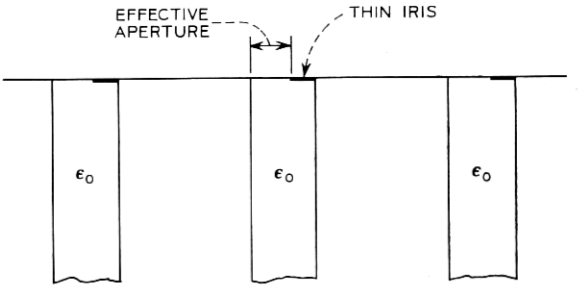

Fig. 4 — Aperture iris geometry.

$$\Phi_{2N} = -\frac{|A_2|}{(|A_1|^2 + |A_2|^2)^{\frac{1}{2}}}\Phi_1 + \frac{A_1^*|A_2|}{A_2^*(|A_1|^2 + |A_2|^2)^{\frac{1}{2}}}\Phi_2 . \quad (25)$$

This redefinition of the first two modes preserves the orthonormality and completeness of the set of waveguide modes while allowing the flexibility in adjusting the desired array excitation. The reflection coefficients which correspond to these redefined modes are R_{1N} and R_{2N}. The polarization characteristics of the radiation pattern may be determined from the θ and ϕ components of the radiated field, E_θ and E_ϕ, respectively. After proper normalization of E_θ and E_ϕ one may obtain the corresponding transmission coefficients[19]

$$T_\theta = \left(\frac{Y'_{002}}{Y_1}\right)^{\frac{1}{2}} \frac{1}{(1 - T_x^2 - T_y^2)^{\frac{1}{2}}} \iint_{\text{(aperture)}} \mathbf{E}_t \cdot (\Psi_{00}^2)^* \, da \quad (26)$$

$$T_\phi = -\left(\frac{Y'_{001}}{Y_1}\right)^{\frac{1}{2}} \iint_{\text{(aperture)}} \mathbf{E}_t \cdot (\Psi_{00}^1)^* \, da \quad (27)$$

where T_x and T_y define the scan angle directional cosines. When the first two waveguide modes are the only propagating ones and while only a single lobe propagates in the free space, equations (24) through (27) are related by the conservation of energy relation:

$$|R_{1N}|^2 + |R_{2N}|^2 + |T_\theta|^2 + |T_\phi|^2 = 1. \quad (28)$$

For more than one lobe in free space or additional propagating modes in the waveguides, (28) has to be accordingly modified.

III. NUMERICAL AND EXPERIMENTAL RESULTS

In order to obtain a numerical solution for the aperture field, the infinite dimensional matrix of equation (15) must be truncated and cast in a finite dimensional form. In other words, the electromagnetic fields will be approximated by a finite Fourier series of the waveguide and free space modes, and consequently the solution of the problem as given by (19), is finite dimensional as well.

In numerical solutions of problems of this type, various ways of ascertaining the validity and accuracy of the solution are desirable. One obvious way is to increase the number of waveguide and free space modes and check the convergence of the solution as a function of the number of modes used in truncating (15). However, for the type of kernel involved in this problem, monotonicity of the convergence is not assured. Nevertheless, convergence is an important check

since this numerical solution is variational or stationary for the impedance.[12, 24] Iterative methods and error estimates[5, 20] may also be used for checking the convergence of the solution. Special symmetries of the reflection coefficients versus the scan angles which are dictated by the array geometry and mode of excitation can serve as a semi-independent check. An important independent check in which the reflection and transmission coefficients can be measured at special scan angles with the aid of a waveguide simulator is used as well.

The numerical results will in general be presented as a function of scan angle. For convenience, however, the differential phase shifts between elements will be used as the independent variables. These quantities are ψ_x in the x-direction and ψ_y in the y-direction. Furthermore, since we limit ourselves to radial planes of scan, we introduce the quantity ψ_r. These quantities are related to the directional cosines as follows:

$$\psi_x = \frac{2\pi b}{\lambda} T_x \; ; \qquad \psi_y = \frac{2\pi d \sin \alpha}{\lambda} T_y \; ; \qquad \psi_r = (\psi_x^2 + \psi_y^2)^{\frac{1}{2}}. \tag{29}$$

The amount of computation can be reduced when one recognizes that the following symmetry in the aperture field as a function of scan exists:

$$\mathbf{E}_t(\psi_x, \psi_y) = \mathbf{E}_t(-\psi_x, -\psi_y). \tag{30}$$

Convergence tests as a function of the number of waveguide and free space modes indicated that 18 waveguide modes and 338 free space modes yield several percent (usually less than 2 percent) accuracy in the magnitude of the reflection coefficients, R_j, except near sharp changes of R_j where the position of the sharp changes is accurate to several degrees in ψ_r.

The energy conservation check, equation (28), is a necessary check but not a sufficient one in this problem as well as in other interior type boundary value problems.[17, 22, 33]

One of various special symmetry checks is depicted in Fig. 5. A square grid array in the (x, y) coordinates is excited by the vertical $\mathrm{TE}_{11}(\mathbf{\Phi}_2)$ mode. In this coordinate system the array parameters are represented in the following way

$$\left.\begin{aligned} a = \text{waveguide radius}; \qquad b = d; \qquad \alpha = 90° \\ \mathbf{\Phi}_{1N} = \mathbf{\Phi}_2 \; ; \qquad \mathbf{\Phi}_{2N} = -\mathbf{\Phi}_1 \end{aligned}\right\}. \tag{31}$$

The parameters of the same array, when viewed in the (x', y') coordi-

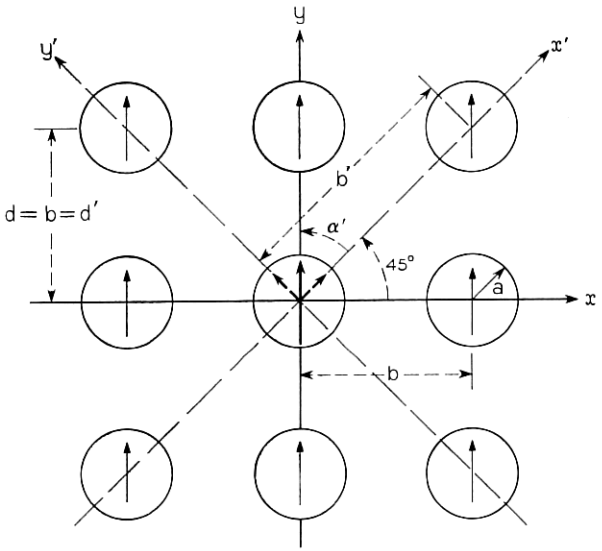

Fig. 5 — Symmetries in square grid arrays.

nate system, can be alternatively represented as

$$\left.\begin{aligned} b' &= (2)^{\frac{1}{2}}d' = (2)^{\frac{1}{2}}d; \qquad \alpha' = 45° \\ \Phi'_{1N} &= \frac{1}{(2)^{\frac{1}{2}}}\{-\Phi'_1 + \Phi'_2\}; \qquad \Phi'_{2N} = \frac{1}{(2)^{\frac{1}{2}}}\{\Phi'_1 + \Phi'_2\} \end{aligned}\right\} \tag{32}$$

where the reference to the (x', y') system is denoted by primes. The same results should be found for this array at any scan direction regardless of the representation. This offers, to a degree, a check on roundoff error. Numerically, the reflection coefficients differed only by a fraction of a percent.

An additional symmetry check is given in Fig. 6, where the magnitudes of the reflection coefficients are plotted versus ψ_r for a 45° plane of scan. R_{1N} and R_{2N} correspond to the reflection coefficients of Φ_{1N} and Φ_{2N} as defined by (31). At $\psi_r = 240°$ (shown by a vertical arrow) the main beam is grazing, while for $\psi_r > 240°$ no beam exists in real space and the total incident power is reflected and divided between the two propagating modes, Φ_{1N} and Φ_{2N}. Of special interest is the point $\psi_r = 180° \times (2)^{\frac{1}{2}} \approx 255°$. At this point $\psi_x = \psi_y = \psi_{t_1} = \psi_{t_2} = 180°$ and the array excitation is as indicated in the inset of Fig. 6. If the array is to be simulated at this scan angle, the appropriate waveguide simulator would

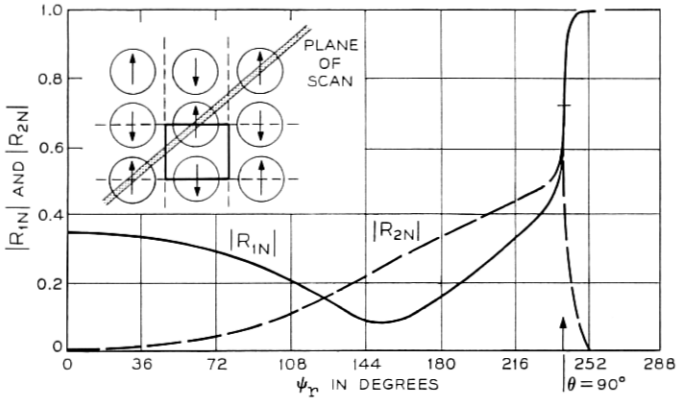

Fig. 6 — Square grid array: $|R_{1N}|$ and $|R_{2N}|$ vs ψ_r in the 45° plane of scan. $\alpha = 0.48$, $b = 1$, $d = 1$, $\lambda = 1.5$ and $\alpha = 90°$.

consist of the square waveguide (solid lines) shown in the inset. It is clear that the horizontal waveguide mode (Φ_{2N}) cannot be excited. The numerical results indeed show that $| R_{2N} | = 0$ at this scan angle.

Figure 7 shows a close agreement between experimental and numerical results for a rectangular grid array with vertical polarization excitation scanned in the H-plane. The scan angle which corresponds to steering phases $\psi_x = \psi_{t_1} = 180°$ and $\psi_y = \psi_{t_2} = 0$, can be simulated

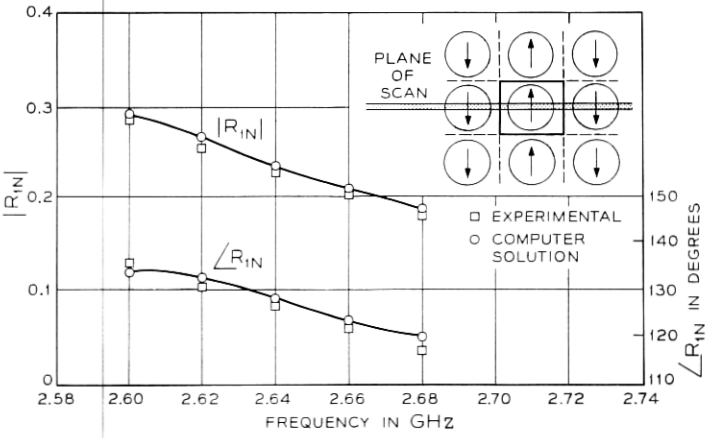

Fig. 7 — Rectangular grid array: computed and experimental results vs frequency at H-plane symmetry point. $a = 3.57$ cm., $b = 16.51$ cm., $d = 8.261$ cm., and $\alpha = 90°$.

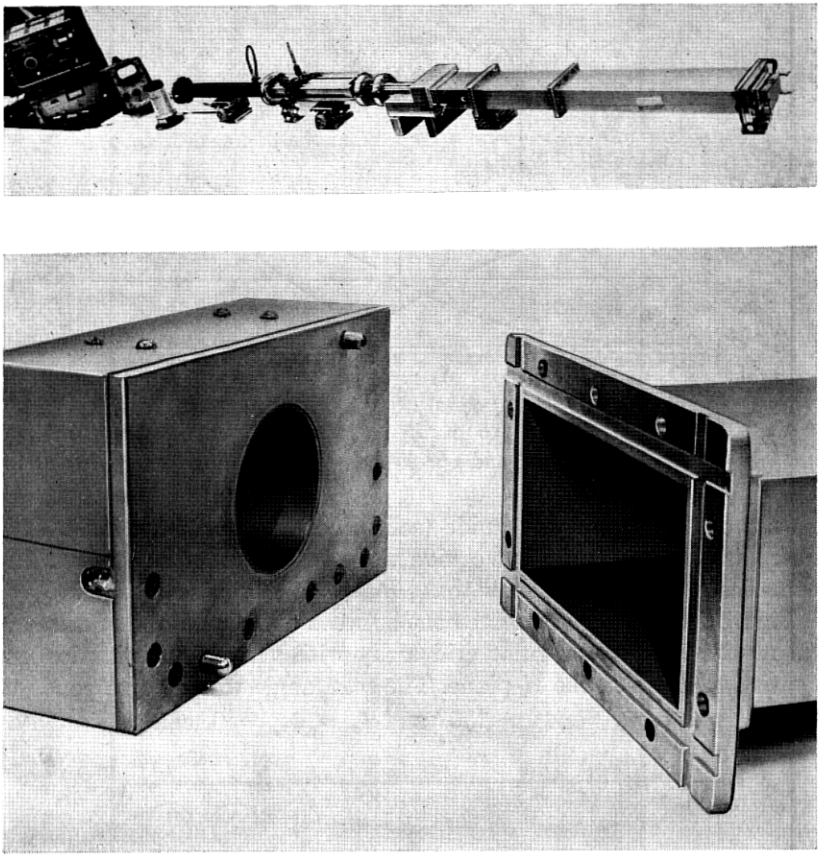

Fig. 8 — Rectangular grid array: simulator for H-plane symmetry point.

by the rectangular waveguide (solid line) in the inset. The experimental results were obtained from measurements of an abrupt junction between a circular waveguide and an L-band rectangular waveguide as shown in Fig. 8.

IV. EQUILATERAL TRIANGLE GRID ARRAYS

Let us consider the reflection and radiation characteristics of circular waveguide arrays arranged in an equilateral triangle grid, and the strong dependence of the array properties upon the mode of excitation. Grating lobe incipience or a beam at grazing is designated by a vertical arrow in the illustrations.

Figure 9 shows the reflection coefficient of an array in the E-plane scan, with vertical polarization excitation. In this plane the horizontal mode is not excited because of symmetry so that $R_{2N} \equiv 0$. As can be seen, the slope of both the magnitude and phase of R_{1N} is discontinuous and singular at a grating lobe incipience, which parallels previous observations in rectangular waveguide arrays.[26, 27] This is related to the asymptotic decay of the coupling coefficients. A forced surface wave resonance can be seen around grating lobe incipience where $|R_{1N}| = 1.0$. Notice that this forced surface wave resonance is extremely sharp and consequently may not be observed in small finite arrays.

The corresponding transmission coefficient T_θ is shown in Fig. 10. The plot of the transmission coefficient is actually the radiation pattern of a single element in the array environment and it exhibits the null which corresponds to a total reflection. Notice that the phase of the transmission coefficient will exhibit a 180° discontinuity when the magnitude has a zero. The magnitude of the reflection coefficients of the same array, in a 60° plane of scan, are shown in Fig. 11. Again,

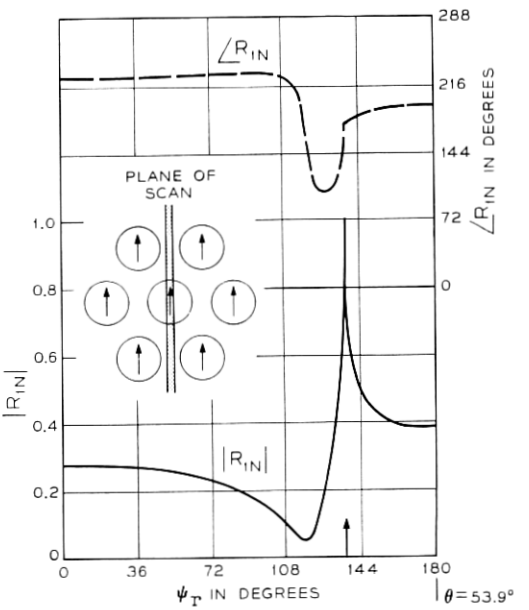

Fig. 9 — E-plane scan of R_{1N} vs ψ_T ($a = 0.48$, $b = 1$, $d = 1$, $\lambda = 1.4$ and $\alpha = 60°$).

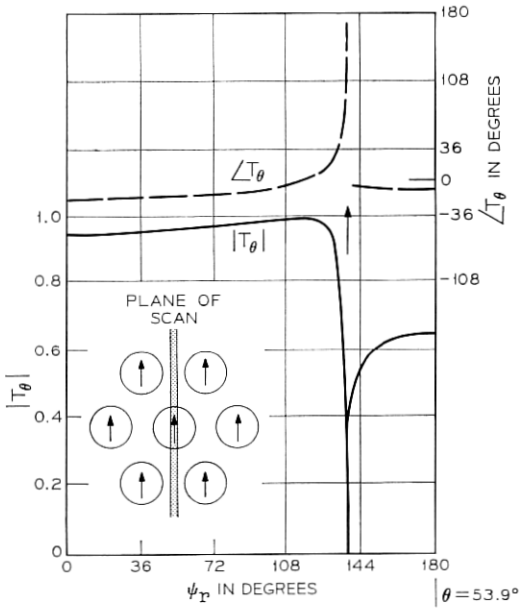

Fig. 10 — E-plane scan of T_θ vs ψ_r ($a = 0.48$, $b = 1$, $d = 1$, $\lambda = 1.4$, and $\alpha = 60°$).

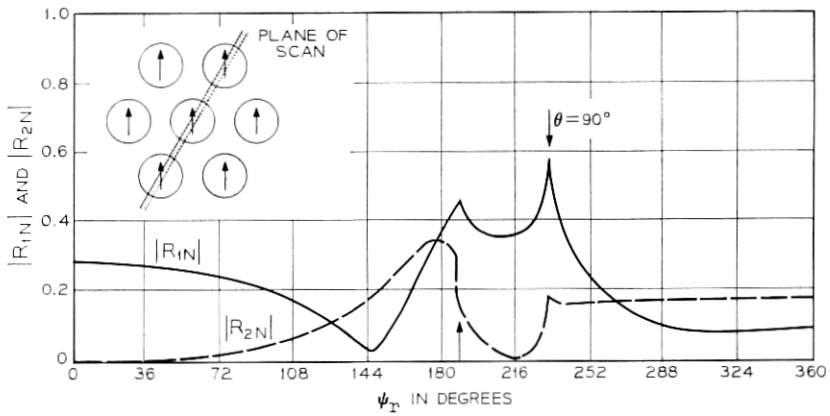

Fig. 11 — $|R_{1N}|$ and $|R_{2N}|$ vs ψ_r in the 60° plane of scan ($a = 0.48$, $b = 1$, $d = 1$, $\lambda = 1.4$, and $\alpha = 60°$).

the singular slope at grating lobe incipience can be observed. As can be seen, the distribution of the reflected power between the two modes is a function of the scan angle.

An interesting phenomenon can be observed in the corresponding transmission characteristics which are shown in Fig. 12. The ϕ trans-

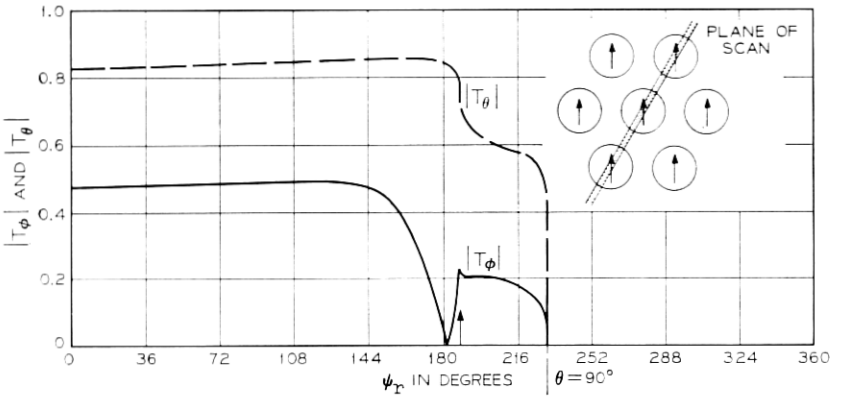

Fig. 12 — $|T_\theta|$ and $|T_\phi|$ vs ψ_r in the 60° plane of scan ($a = 0.48$, $b = 1$, $d = 1$, $\lambda = 1.4$, and $\alpha = 60°$).

mission coefficient, T_ϕ, vanishes prior to grating lobe incipience (the positions of the vertical arrows). The vanishing of T_ϕ at this scan angle can be directly related, when coupled with the vector symmetries in the array excitation and geometry, to a forced surface wave resonance. If the array excitation consists of the sum of the two modes (equal in phase and magnitude) indicated by the solid arrows in Fig. 13, then in the 60° scan plane $T_\theta \equiv 0$ by symmetry considerations and T_ϕ vanishes as shown in Fig. 12. Since the vectorial sum of the two solid arrows in Fig. 13 is the dashed arrow, zero transmission or a forced surface wave resonance will occur in the H-plane of this polarization. Figs. 14 and 15 indeed show this effect in the H-plane scan where $|R_{1N}|$ and $|T_\phi|$ attain unity and zero respectively prior to grating lobe incipience.*

Since the forced surface waves are related to the vector symmetries just mentioned, one may anticipate that the scan points at which they occur are isolated. Figure 16 indeed demonstrates that the forced resonances in the E and H planes occur at isolated points. The scan around

* The difference in the values of ψ_r at which these phenomena occur is inherent in the definition of ψ_r, equation (20).

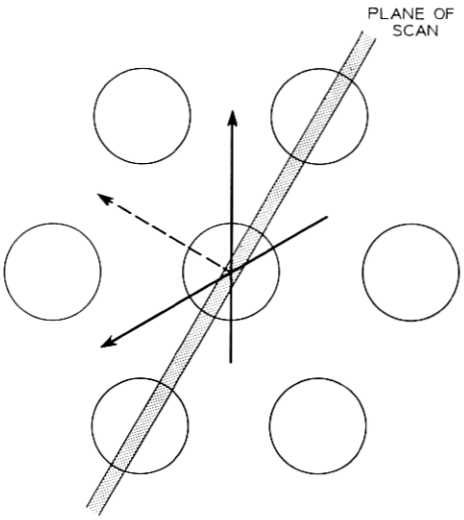

Fig. 13 — Vector symmetry relationships between transmission zeros and forced surface waves.

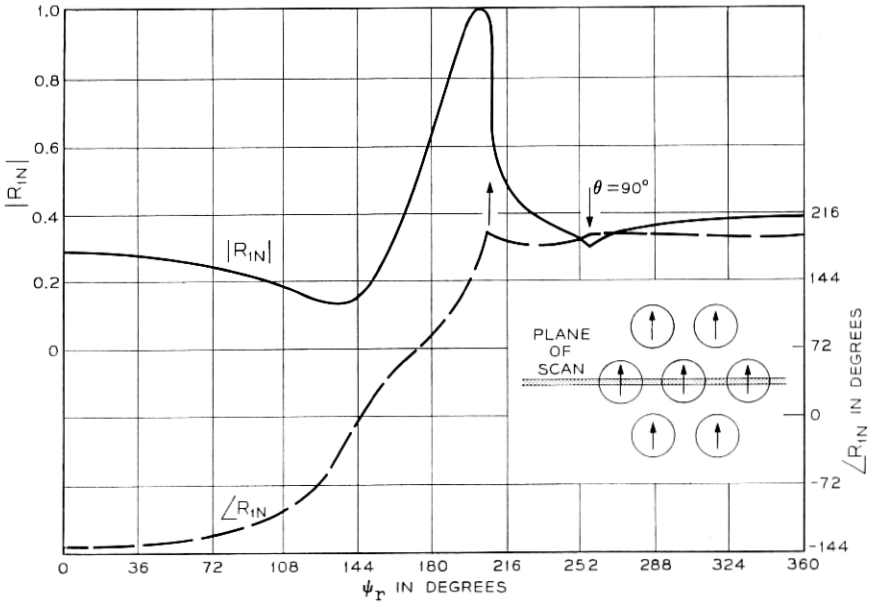

Fig. 14 — H-plane scan of R_{1N} vs ψ_r ($a = 0.48$, $b = 1$, $d = 1$, $\lambda = 1.4$, and $\alpha = 60°$)

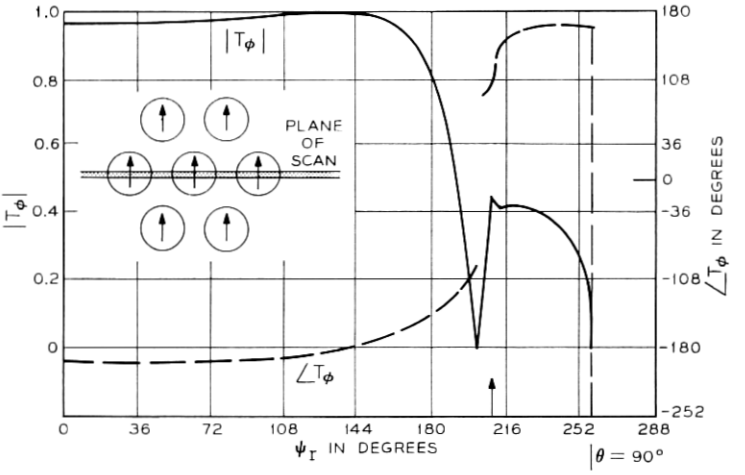

Fig. 15 — H-plane scan of T_ϕ vs ψ_r ($a = 0.48$, $b = 1$, $d = 1$, $\lambda = 1.4$, and $\alpha = 60°$).

the grating lobe circles in Fig. 17 shows that the peak of the *total* reflection $|R_T| = (|R_{1N}|^2 + |R_{2N}|^2)^{\frac{1}{2}}$ varies from unity in the H plane ($\delta = 0$), gradually decreases, and then increases again and reaches unity in the E-plane ($\delta = 90°$). The anomalous behavior near grating lobe incipience is eliminated when the polarization of the excitation is changed to horizontal, as shown in Fig. 17, indicating thus the strong dependence of the forced surface wave resonances upon the mode of excitation. Over the frequency band given by $1.3 \leqq \lambda \leqq 1.5$, qualitatively similar behavior of the radiation and reflection characteristics of the array was observed.

Figure 18 shows the reflection characteristics of the array under circular polarization excitation. In this case

$$\mathbf{\Phi}_{1N} = -\frac{1}{(2)^{\frac{1}{2}}}\{\mathbf{\Phi}_1 + i\mathbf{\Phi}_2\}; \qquad \mathbf{\Phi}_{2N} = -\frac{1}{(2)^{\frac{1}{2}}}\{\mathbf{\Phi}_1 - i\mathbf{\Phi}_2\}. \quad (33)$$

The incident mode is $\mathbf{\Phi}_{1N}$.

Again the singular slope of these curves at grating lobe incipience can be seen. The division of the reflected power between the two modes as a function of scan may be observed as well. Fig. 19 shows the polarization characteristics of the radiation pattern of an array element. The axial ratio, denoted as $A.R.$, is the ratio of the minor to major axis of the polarization ellipse while the tilt angle of the major axis, τ, is taken with respect to the ϕ axis. As indicated by

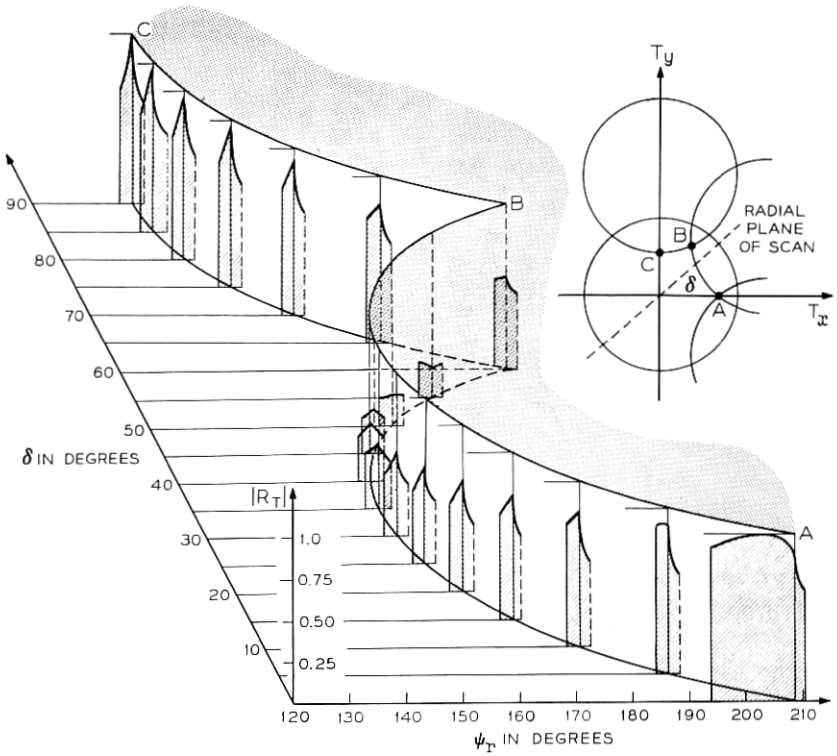

Fig. 16 — $|R_T|$ vs ψ_T in the vicinity of grating lobe incipience.

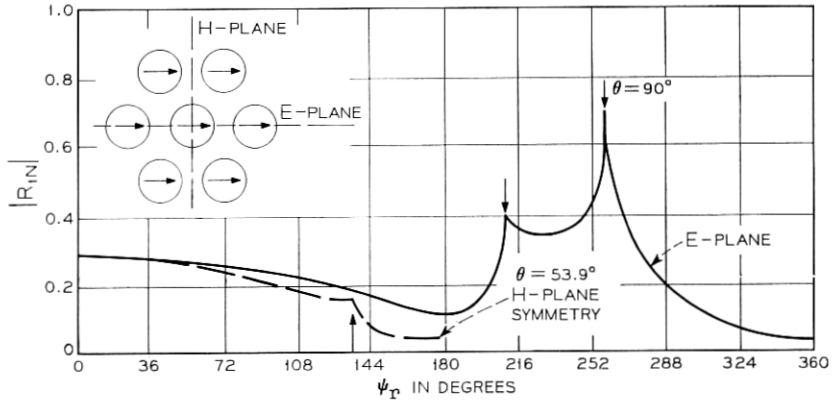

Fig. 17 — E- and H-plane scans of $|R_{1N}|$ vs ψ_T for horizontal polarization ($a = 0.48$, $b = 1$, $d = 1$, $\lambda = 1.4$, and $\alpha = 60°$).

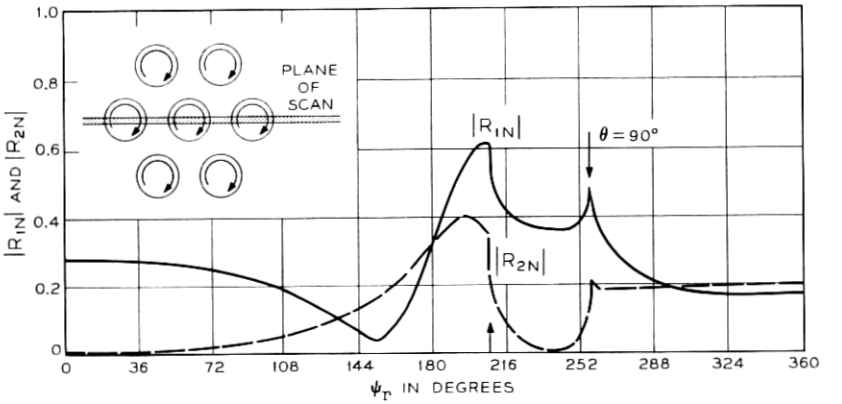

Fig. 18 — $|R_{1N}|$ and $|R_{2N}|$ vs ψ_r in the 0° plane of scan. Circularly polarized excitation ($a = 0.48$, $b = 1$, $d = 1$, $\lambda = 1.4$, and $\alpha = 60°$).

the plot, the element (or the array) far field pattern is circularly polarized around broadside, $A.R. = 1.0$. It deteriorates to linear polarization, $A.R. = 0$, at two points prior to grating lobe incipience. The linear polarization at $\psi_r = 203.5°$ with $\tau = 90°$ results from the H-plane forced surface wave resonance of Figs. 14 and 15 where T_ϕ vanishes. The null of the axial ratio at $\psi_r = 207°$ (with $\tau = 105°$)

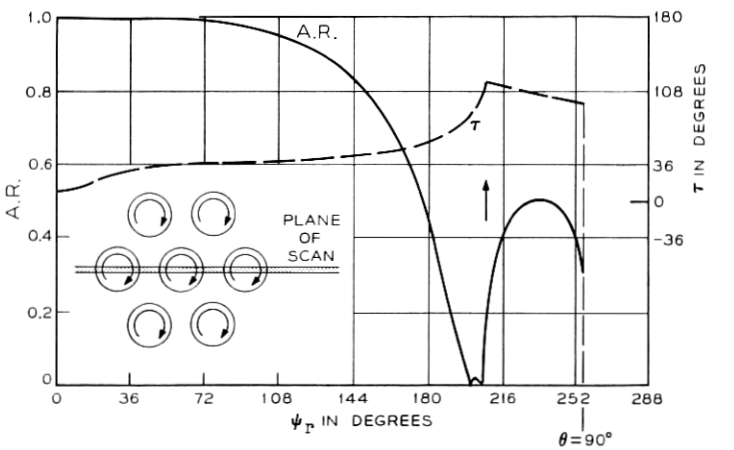

Fig. 19 — Radiated axial ratio (A.R.) and tilt angle (τ) vs ψ_r in the 0° plane of scan. Circularly polarized excitation ($a = 0.48$, $b = 1$, $d = 1$, $\lambda = 1.4$, and $\alpha = 60°$).

is caused by the difference between the phases of T_θ and T_ϕ causing the ϕ and θ components of the far field to be in phase.

The reflection and polarization characteristics in the 30° plane of scan are shown in Figs. 20 and 21, respectively. In this case the single null of the axial ratio at grating lobe incipience results from the E-plane forced surface wave resonance of Figs. 9 and 10. For planes of scan between 0° and 30° the results corresponding to one plane change gradually to those of the other plane. Around grating lobe incipience the axial ratio drops appreciably (to around 0.1) but does not reach zero. From the circular symmetry of excitation and six-fold symmetry of the array geometry, a 30° sector of scan completely specifies the array reflection and radiation characteristics.

V. CONCLUSIONS

A general formulation of the planar phased array boundary value problem has been given in terms of a vector two dimensional integral equation. The solution of this equation by the Ritz-Galerkin method closely agreed with experimental results.

Equilateral triangle phased arrays of circular waveguides were numerically analyzed. It was found that forced aperture resonances or forced surface waves, manifested by total reflection and no radiation, do exist for these arrays even in the absence of dielectric materials. These effects were observed over a 15 per cent frequency band. The forced aperture resonances occurred prior or close to grat-

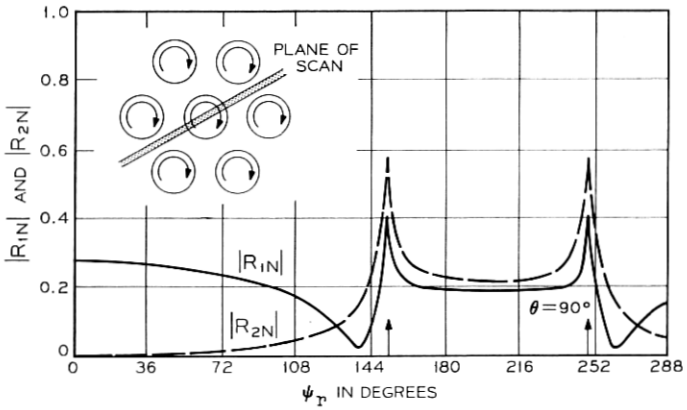

Fig. 20 — $|R_{1N}|$ and $|R_{2N}|$ vs ψ_r in the 30° plane of scan. Circularly polarized excitation ($a = 0.48$, $b = 1$, $d = 1.\lambda = 1.4$, and $\alpha = 60°$).

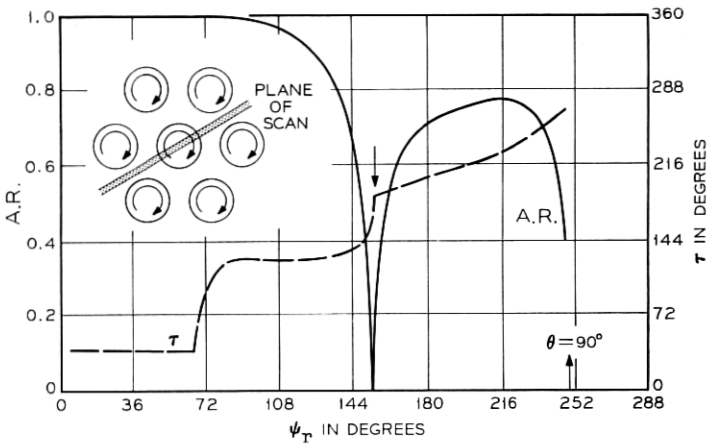

Fig. 21 — Radiated axial ratio (A.R.) and tilt angle (τ) vs ψ_T in the 30° plane of scan. Circularly polarized excitation ($a = 0.48$, $b = 1$, $d = 1$, $\lambda = 1.4$, and $\alpha = 60°$).

ing lobe incipience in the E and H plane of scan for vertical polarization excitation. These resonances were found to occur at isolated points as a function of the scan variables and are strongly influenced by the mode of excitation. The resonances vanish when the polarization of excitation changes from vertical to horizontal.

The polarization characteristics of the radiation pattern (or alternatively the radiation pattern of a single excited element in the array environment) is shown at selected planes of scan for circular polarization excitation. The degradation of the axial ratio resulting from the forced surface waves was shown. Total reflection or no transmission owing to forced aperture resonances were not observed for circular polarization excitation in the cases presented.

The analysis of coaxial waveguide arrays, as well as the incorporation of thin, circularly symmetric irises in the aperture of the waveguide element, can be carried out along lines similar to those discussed here.

The effects of dielectric loading of the array as well as dielectric covers and plugs have also been studied.[34]

VI. ACKNOWLEDGMENTS

The invaluable assistance of Mr. S. Renna and Miss A. M. Russell in the computations, and Messrs. P. E. Butzien and L. H. Hendler in the experimental measurements, are gratefully acknowledged. The

authors would like to thank Dr. C. P. Wu, Dr. J. A. Cochran, and Dr. E. R. Nagelberg for their helpful suggestions.

APPENDIX A

Floquet Type Wave Functions in Skewed Coordinates

Consider the periodic array, Figs. 1 and 2, excited with incremental phase shifts (steering phases) between adjacent cells along the s_1 and s_2 coordinates. A complete set of solutions to the scalar wave equation, each of which varies periodically, according to Floquet's theorem, along the s_1 and s_2 coordinates is

$$S_{mn} = \exp(iB_{mn}z) \exp i\left[\frac{\psi_{t_1}}{b} - \frac{2\pi m}{b}\right]s_1 \exp i\left[\frac{\psi_{t_2}}{d} - \frac{2\pi n}{d}\right]s_2 \qquad (34)$$

with the integers $m, n = -\infty, \ldots -1, 0, 1, 2, 3, \ldots, +\infty$. Equation (34) describes a wave traveling (or decaying) in the z direction with propagation constant B_{mn} (exp $-i\omega t$ time convention). The steering phases ψ_{t_1} and ψ_{t_2} are directly related to the beam pointing direction, $\hat{r}$, of a radiated plane wave with a vector propagation constant $\mathbf{k}_0 = k_0\hat{r}$, so that (34) can be rewritten as

$$S_{mn} = \exp(iB_{mn}z) \exp i\left[\mathbf{k}_0 \cdot \hat{s}_1 - \frac{2\pi m}{b}\right]s_1 \exp i\left[\mathbf{k}_0 \cdot \hat{s}_2 - \frac{2\pi n}{d}\right]s_2 . \qquad (35)$$

The free space propagation vector $\mathbf{k}_0$ can be expressed in the cartesian coordinate system as

$$\mathbf{k}_0 = k_0[T_x\hat{x} + T_y\hat{y} + T_z\hat{z}] \qquad (36)$$

where T_x, T_y and T_z are the directional cosines of $\mathbf{k}_0$ with respect to that system and $\hat{x}$, $\hat{y}$, and $\hat{z}$ are the unit vectors. The quantities

$$\mathbf{k}_0 \cdot \hat{s}_1 = \frac{\psi_{t_1}}{b} \quad \text{and} \quad \mathbf{k}_0 \cdot \hat{s}_2 = \frac{\psi_{t_2}}{d} \qquad (37)$$

are the projections of $\mathbf{k}_0$ on the reciprocal grid (lattice) coordinates t_1 and t_2, respectively.[15,28-30] The unit vectors in the t_1 and t_2 directions form a biorthogonal set with $\hat{s}_1$ and $\hat{s}_2$ (Fig. 22). To express (35) in cartesian coordinates it can easily be shown that

$$s_1 = x - y \cot \alpha, \qquad s_2 = y/\sin \alpha, \qquad (38)$$

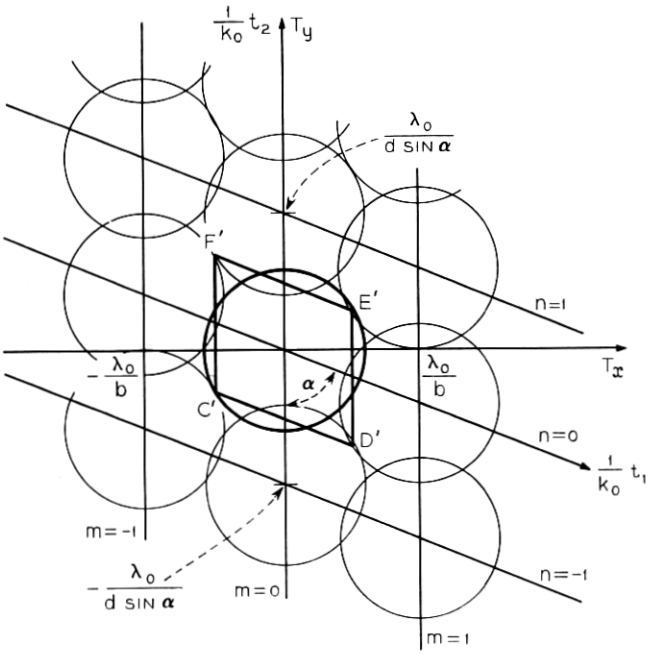

Fig. 22 — Grating lobe diagram in reciprocal lattice coordinates.

so that the substitution of (38) into (35) yields

$$S_{mn} = \exp(iB_{mn}z) \exp i\left[k_0 T_x - \frac{2\pi m}{b}\right]x \cdot \exp i\left[k_0 T_y - \left(\frac{2\pi n}{d \sin \alpha} - \frac{2\pi m}{b \tan \alpha}\right)\right]y. \quad (39)$$

The propagation constants of the (m, n)th Floquet mode along the x and y directions, k_x and k_y respectively, are

$$\begin{aligned} k_x &\equiv \mathbf{k} \cdot \hat{x} = k_0 T_x - \frac{2\pi m}{b}; \\ k_y &\equiv \mathbf{k} \cdot \hat{y} = k_0 T_y - \left(\frac{2\pi n}{d \sin \alpha} - \frac{2\pi m}{b \tan \alpha}\right). \end{aligned} \quad (40)$$

Since S_{mn} is a solution to the scalar wave equation, it can be shown that

$$B_{mn} = (k_0^2 - k_x^2 - k_y^2)^{\frac{1}{2}} = \left\{k_0^2 - \left[k_0 T_x - \frac{2\pi m}{b}\right]^2 - \left[k_0 T_y - \left(\frac{2\pi n}{d \sin \alpha} - \frac{2\pi m}{b \tan \alpha}\right)\right]^2\right\}^{\frac{1}{2}} \tag{41}$$

where the positive imaginary root holds for $(k_x^2 + k_y^2) > k_0^2$ (time convention exp $-i\omega t$).

Each mode, S_{mn}, for which B_{mn} is real corresponds to a radiated plane wave of the phased array. The plane wave with the indices $m = 0$ and $n = 0$ is identified with the main beam while m or $n \neq 0$ corresponds to a radiating grating lobe. As a function of T_x and T_y (or ψ_{t_1} and ψ_{t_2}), a given B_{mn} may become pure imaginary as it goes through a zero, as in equation (41). In such cases, the related Floquet mode, S_{mn}, becomes evanescent or nonradiating. By plotting the curves obtained by setting the $B_{mn} = 0$ as a function of T_x and T_y, one obtains a convenient diagram which illustrates these effects. Setting $B_{mn} = 0$ yields

$$\left[T_x - \frac{m\lambda_0}{b}\right]^2 + \left[T_y - \left(\frac{n\lambda_0}{d \sin \alpha} - \frac{m\lambda_0}{b \tan \alpha}\right)\right]^2 = 1, \tag{42}$$

where $\lambda_0 = 2\pi/k_0$. As a function of T_x and T_y, (42) represents a family of circles with unit radius displaced from the origin. This diagram of displaced circles constitutes the well-known grating lobe diagram, Fig. 22.[31, 32]

Notice that the steering phases, ψ_{t1} and ψ_{t2}, are related to T_x and T_y through equations (36) and (37). The parallelogram $C'D'E'F'$ of Fig. 22 corresponds to the range of steering phases

$$-\pi \leqq \psi_{t_1} \leqq \pi; \qquad -\pi \leqq \psi_{t_2} \leqq \pi \tag{43}$$

and is a periodic cell along the t_1 and t_2 coordinates.

As mentioned in Section II, it is possible to define a complete orthonormal set[16] of vector modes $\{\Psi_{mn}^{p}\}$ over the parallelogram $CDEF$, Fig. 2. The tangential electromagnetic field at the plane $z = 0^+$ can be expressed by a Fourier series of this set of modes which consists of both TE and TM modes (transverse to z). These modes, $\{\Psi_{mn}^{\mathrm{TE}}\}$ and $\{\Psi_{mn}^{\mathrm{TM}}\}$, are given by

$$\Psi_{mn}^{\mathrm{TE}} = \frac{\exp i(xk_x + yk_y)}{(bd \sin \alpha)^{\frac{1}{2}}} \left\{\frac{k_y}{k_r}\hat{x} - \frac{k_x}{k_r}\hat{y}\right\}\Bigg|_{m,n} \tag{44}$$

and

$$\Psi_{mn}^{\mathrm{TM}} = \frac{\exp i(xk_x + yk_y)}{(bd \sin \alpha)^{\frac{1}{2}}} \left\{\frac{k_x}{k_r}\hat{x} + \frac{k_y}{k_r}\hat{y}\right\}\Bigg|_{m,n} \tag{45}$$

with $k_r = (k_x^2 + k_y^2)^{\frac{1}{2}}$. The quantities k_x and k_y are functions of (m, n) as given by (40). The orthonormality of this set of vector modes is defined by the following scalar products:

$$\langle \Psi_{mn}^{\mathrm{TE}}, \Psi_{pq}^{\mathrm{TE}} \rangle = \iint_{\substack{\text{parallelogram} \\ CDEF}} \Psi_{mn}^{\mathrm{TE}} \cdot (\Psi_{pq}^{\mathrm{TE}})^* \, dx \, dy = \delta_{mn,pq} , \tag{46}$$

where

$$\delta_{mn,pq} = \begin{cases} 1 & \text{for} \quad m = p \quad \text{and} \quad n = q, \\ 0 & \text{otherwise} \end{cases} \tag{47}$$

$$\langle \Psi_{mn}^{\mathrm{TE}}, \Psi_{pq}^{\mathrm{TM}} \rangle = 0 \tag{48}$$

and

$$\langle \Psi_{mn}^{\mathrm{TM}}, \Psi_{pq}^{\mathrm{TM}} \rangle = \delta_{mn,pq} . \tag{49}$$

APPENDIX B

On the Invariance of the Scalar Product with the Shape of the Periodic Cell

The orthonormality and completeness of the set $\{\Psi_{mn}^{p}\}$ of Floquet modes, equations (44) and (45), need not be defined over a specific periodic cell such as the parallelogram $CDEF$ of Fig. 2. This fact is especially significant when a periodic cell intercepts parts of more than one circular (or other type of element) aperture. It will be shown that the orthonormality of $\{\Psi_{mn}^{p}\}$ can be preserved over a properly deformed periodic cell which contains only a single waveguide aperture.

Using (37), equation (44) can be rewritten as

$$\Psi_{mn}^{\mathrm{TE}} = \mathbf{F}(m, n) \exp i\left[\frac{\psi_{t_1} - 2\pi m}{b} s_1 + \frac{\psi_{t_2} - 2\pi n}{d} s_2\right] . \tag{50}$$

The scalar product betewen two TE modes is

$$\begin{aligned} \langle \Psi_{mn}^{\mathrm{TE}}, \Psi_{pq}^{\mathrm{TE}} \rangle &= \delta_{mn,pq} \\ &= \iint_{(CDEF)} \Psi_{mn}^{\mathrm{TE}} \cdot (\Psi_{pq}^{\mathrm{TE}})^* \, dx \, dy \\ &= \iint_{(CDEF)} \Psi_{mn}^{\mathrm{TE}} \cdot (\Psi_{pq}^{\mathrm{TE}})^* \sin \alpha \, ds_1 \, ds_2 \\ &= \mathbf{F}(m, n) \cdot \mathbf{F}(pq)^* \sin \alpha \end{aligned} \tag{51}$$

$$\cdot \iint_{(CDEF)} \exp -i\left[\frac{2\pi(m-p)}{b}\, s_1 + \frac{2\pi(n-q)}{d}\, s_2\right] ds_1\, ds_2 \,.$$

The integral over the parallelogram $CDEF$ in (51) can be divided into three (or more) integrals over the triangles CGK and LEI and the polygon $GDLIFK$ (Fig. 2):

$$\iint_{CDEF} = \iint_{CGK} + \iint_{LEI} + \iint_{GDLIFK} . \tag{52}$$

Because of the array periodicity, the triangles DHL and LEI are displaced by b with respect to the triangles CGK and KFJ, respectively, along the s_1 direction. Thus, for example, if the s_1 coordinate of the points within the triangle DHL is s_1' given by

$$s_1' = s_1 + b \qquad \text{with} \qquad ds_1' = ds_1 \tag{53}$$

then

$$\iint_{DHL} \exp -i\left[\frac{2\pi(m-p)}{b}\, s_1' + \frac{2\pi(n-q)}{d}\, s_2\right] ds_1'\, ds_2$$

$$= \exp -i2\pi(m-p) \iint_{CGK} \exp -i\left[\frac{2\pi(m-p)}{b}\, s_1 + \frac{2\pi(n-q)}{d}\, s_2\right] ds_1\, ds_2$$

$$= \iint_{CGK} \exp -i\left[\frac{2\pi(m-p)}{b}\, s_1 + \frac{2\pi(n-q)}{d}\, s_2\right] ds_1\, ds_2 \,. \tag{54}$$

Similarly

$$\iint_{LEI} \exp -i\left[\frac{2\pi(m-p)}{b}\, s_1 + \frac{2\pi(n-q)}{d}\, s_2\right] ds_1\, ds_2$$

$$= \iint_{KFJ} \exp -i\left[\frac{2\pi(m-p)}{b}\, s_1 + \frac{2\pi(n-q)}{d}\, s_2\right] us_1\, ds_2. \tag{55}$$

Thus

$$\iint_{CDEF} \exp -i\left[\frac{2\pi(m-p)}{b}\, s_1 + \frac{2\pi(n-q)}{d}\, s_2\right] ds_1\, ds_2$$

$$= \iint_{GHIJ} \exp -i\left[\frac{2\pi(m-p)}{b}\, s_1 + \frac{2\pi(n-q)}{d}\, s_2\right] ds_1\, ds_2 \tag{56}$$

and the orthonormality and completeness of the set $\{\Psi^{p}_{mn}\}$ is preserved over the new periodic cell $GHIJ$. This is the two dimensional analog of the single dimensional Fourier series whereby the functions and coefficients are independent of the initial value of the period. In fact, the two dimensional periodic cell can be deformed to any shape which contains a single waveguide provided that the area of the cell stays the same and the parts of the cell which cause the deformation are translated by b or d along the s_1 and s_2 coordinates, respectively.

REFERENCES

1. Galindo, V. and Wu, C. P., "Numerical Solutions for an Infinite Phased Array of Rectangular Waveguides with Thick Walls," IEEE Trans. Antennas and Propagation, *AP-14,* No. 2 (March 1966), pp. 149–158.
2. Wu, C. P. and Galindo, V., "Properties of a Phased Array of Rectangular Waveguides with Thin Walls," IEEE Trans. on Antennas and Propagation," *AP-14,* No. 2 (March 1966), pp. 163–173.
3. Wu, C. P. and Galindo, V., "Surface-Wave Effects on Dielectric Sheathed phased Arrays of Rectangular Waveguides," B.S.T.J., *47,* No. 1, (January 1968), pp. 117–142.
4. Wu, C. P. and Galindo, V., "Surface-Wave Effects on Phased Arrays of Rectangular Waveguides Loaded with Dielectric Plugs," IEEE Trans. Antennas and Propagation, *AP-16,* No. 3 (May 1968), pp. 358–360.
5. Amitay, N. and Galindo, V., "Application of a New Method for Approximate Solutions and Errors Estimates to Waveguide Discontinuity and Phased Array Problems," *Radio Science, 3,* No. 8 (August 1968), pp. 830–844.
6. Amitay, N., Cook, J. S., Pecina, R. G., and Wu, C. P., "On Mutual Coupling and Matching Conditions in Large Planar Phased Arrays," Proc. 1964 IEEE Antennas and Propagation Int. Symp., L. I., N. Y., September 1964, pp. 150–156.
7. Lechtreck, L. W., "Effects of Coupling Accumulation in Antenna Arrays," IEEE Trans. Antennas and Propagation, *AP-16,* No. 1 (January 1968), pp. 31–37.
8. Farrell, G. F., Jr. and Kuhn, D. H., "Mutual Coupling Effects of Triangular-Grid Arrays by Modal Analysis," IEEE Trans. Antennas and Propagation, *AP-14,* No. 5 (September 1966), pp. 652–654.
9. Diamond, B. L., "Resonance Phenomena in Waveguide Arrays," Proc. 1967 IEEE Antennas and Propagation Int. Symp., Ann Arbor, Mich., October 1967, pp. 110–115.
10. Galindo, V., "A Generalized Approach to a Solution of Aperiodic Arrays and Modulated Surfaces," IEEE Trans. Antennas and Propagation, *AP-16,* No. 4 (July 1968), pp. 424–430.
11. Collin, R. E., *Field Theory of Guided Waves,* New York: McGraw-Hill, 1960, pp. 430–441 and pp. 465–468.
12. Galindo, V. and Wu, C. P., "Integral Equations and Variational Expressions for Arbitrary Scanning of Regular Infinite Arrays," IEEE Trans. Antenas and Propagation, *AP-14,* No. 3, (May 1966), pp. 392–394.
13. Hannan, P. W., and Balfour, M. A., "Simulation of a Phased-Array Antenna in Waveguide," IEEE Trans. Antennas and Propagation, *AP-13,* No. 3 (May 1965), pp. 342–353.
14. Balfour, M. A., "Phased Array Simulators in Waveguide for Triangular Arrangement of Elements," IEEE Trans. Antennas and Propagation, *AP-13,* No. 3, (May 1965), pp. 475–476.
15. Brillouin, L., *Wave Propagation in Periodic Structures,* New York: Dover Publications, 1953, pp. 94–121.

16. *Waveguide Handbook,* ed. N. Marcuvitz, Radiation Laboratory Series., vol. 10, New York: McGraw-Hill, 1951.
17. Titchmarsh, E. C., *The Theory of Functions,* London: Oxford University Press, 1939, pp. 43–45.
18. Kantorovich, L. V. and Krylov, V. I., *Approximate Methods of Higher Analysis,* New York: Interscience Publishers, 1964.
19. Amitay, N. and Galindo, V., "On the Scalar Product of Certain Circular and Cartesian Wave Functions," IEEE Trans. Microwave Theory and Techniques, *MTT-16,* No. 4, (April 1968), pp. 265–266.
20. Cole, W. J., Nagelberg, E. R., and Nagel, C. M., "Iterative Solution of Waveguide Discontinuity Problems," B.S.T.J., *46,* No. 3 (March 1967), pp. 649–672.
21. Galindo, V. and Wu, C. P., "The Relation Between the Far-Zone Pattern of the Singly Exited Element and the Transmission Coefficient of the Principle Lobe in an Infinite Array," IEEE Trans. Antennas and Propagation, *AP-14,* No. 3 (May 1966), pp. 397–398.
22. Amitay, N. and Galindo, V., "A Note on the Radiation Characteristics and Forced Surface Wave Phenomena in Triangular Grid Circular Waveguide Phased Arrays," scheduled to be published in IEEE Trans. Antennas and Propagation, *AP-16,* No. 6 (November 1968).
23. Galindo, V. and Wu, C. P., "Dielectric Loaded and Covered Rectangular Waveguide Phased Arrays," B.S.T.J., *47,* No. 1 (January 1968), pp. 93–116.
24. Wu, C. P., "Note on Integral Equations and Variational Expressions for Arbitrary Scanning of Regular Infinite Arrays," IEEE Trans. Antennas and Propagation, *AP-16,* No. 1 (January 1968), pp. 136–138.
25. Lee, S. W., "Radiation from an Infinite Array of Parallel-Plate Waveguides with Thick Walls," IEEE Trans. Microwave Theory and Techniques, *MTT-15,* No. 6 (June 1967), pp. 364–371.
26. Galindo, V. and Wu, C. P., "Asymptotic Behavior of the Coupling Coefficients for an Infinite Array of Thin-Walled Rectangular Waveguides," IEEE Trans. Antennas and Propagation, *AP-14,* No. 2 (March 1966), pp. 248–249.
27. Galindo, V. and Wu, C. P., "On the Asymptotic Decay of Coupling for Infinite Phased Arrays," Int. Sci. Radio Union, Washington, D. C., Spring 1966.
28. Kahn, W. K., "Ideal Efficiency of a Radiating Element in an Infinite Array," IEEE Trans. Antennas and Propagation, *AP-15,* No. 4 (July 1967), pp. 534–542.
29. Borgiotti, G. V., "Impedance and Gain of a Dipole in an Infinite Periodic Phased Array," Research Triangle Institute, Durham, N. C., Technical Report TRR-25 (March 4, 1966).
30. Dufort, E. C., "Finite Scattering Matrix for an Infinite Antenna Array," Radio Science, *2,* No. 1 (January 1967), pp. 19–27.
31. Blass, J. and Rabinowitz, S. J., "Mutual Coupling in Two-Dimensional Arrays," IRE Wescon Convention Record, *1,* pt. 1 (1957), pp. 134–139.
32. von Aulock, W. H., "Properties of Phased Arrays," Proceedings IRE, *48,* No. 10 (October 1960), pp. 1715–1727.
33. Amitay, N. and Galindo, V., "On Energy Conservation and the Method of Moments in Scattering Problems," to be published.
34. Amitay, N. and Galindo, V., "Characteristics of Dielectric Covered and Loaded Circular Waveguide Phased Arrays," Proc. Int. Sci. Radio Union, Boston, Mass., September 1968.